Chandra Observation of the X-Ray Source Population of NGC 6946

S. S. Holt[1], E. M. Schlegel[2], U. Hwang[3], and R. Petre[3]

ABSTRACT

We present the results of a study of discrete X-ray sources in NGC 6946 using a deep *Chandra* ACIS observation. Based on the slope of the log N-log S distribution and the general correlation of sources with the spiral arms, we infer that the overall discrete source sample in NGC 6946 is dominated by high mass X-ray binaries, in contrast to the source distributions in M31 and the Milky Way. This is consistent with the higher star formation rate in NGC 6946 than in those galaxies. We find that the strong X-ray sources in the region of the galactic center do not correlate in detail with images of the region in the near-IR, although one of them may be coincident with the galactic center. The non-central ultra-luminous X-ray source in NGC 6946, previously identified with a supernova remnant, has an X-ray spectrum and luminosity that is inconsistent with either a traditional pulsar wind nebula or a blast wave remnant.

Subject headings: X-ray sources, X-ray binaries, high-mass X-ray binaries, galaxies

1. Introduction

NGC 6946 is a relatively nearby grand-design spiral galaxy. It has been classified as having strong nuclear starburst activity (Elmegreen, Chromey, & Santos 1998), and the six historical supernova remnants recorded during the past century attest to a high rate of star formation in its spiral arms (Sauty, Gerin, & Casoli 1998). Its face-on aspect provides the opportunity to observe the total X-ray source population of a spiral galaxy and to compare its characteristics with those of other nearby spiral galaxies.

The distance to NGC 6946 is estimated between 5.1 Mpc (deVaucouleurs 1979) and 5.9 Mpc (Karachentsev, Sharina, & Huchtmeier 2000). We adopt 5.9 Mpc (see Larsen et al. 2002), so that our luminosity estimates would be reduced by one-quarter for a distance of 5.1 Mpc. The low galactic inclination of NGC 6946 indicates that the preponderance of photoelectric absorption in its direction arises from gas in the Milky Way. From the extinction maps of (Schlegel, Finkbeiner, & Davis 1998), the average hydrogen column density in the direction of NGC 6946 should be N_H = 3-5$\times 10^{21}$ cm^{-2}.

Several recent studies of NGC 6946 have been devoted to its X-ray source, radio source and supernova remnant populations. Schlegel (1994) and Schlegel, Blair, & Fesen (2000) detected a total of fourteen X-ray sources with *Einstein*, *Rosat* and *ASCA*, four of which were coincident with entries in the 118-member radio source catalog of Lacey, Duric, & Goss (1997)(hereafter LDG). Lacey & Duric (2001) invoked the simple requirement of a nonthermal radio spectrum to identify 35 members of the LDG catalog that can be considered "middle-aged" (i.e., $\sim 10^4$ years) supernova remnants. Of these, there is only one match with the 27-member optically selected SNR catalog of Matonick & Fesen (1997); this single coincidence (hereafter

[1]Olin College, Needham, MA

[2]Center for Astrophysics, SAO/HCO, Cambridge, MA

[3]Laboratory for High Energy Astrophysics, GSFC, Greenbelt, MD

MF16) was further identified with the strongest X-ray source in NGC 6946 detected by Schlegel, Blair, & Fesen (2000).

In this paper we use X-ray imaging and spectral data from the *Chandra* observatory to study the X-ray source population of this face-on spiral galaxy in terms of its logN-logS distribution, spatial distribution, and spectral distribution. We compare these properties to those of other spiral galaxies with varying star formation rates.

2. Source Detection with *Chandra*

NGC 6946 was observed by the ACIS instrument aboard the *Chandra Observatory* for approximately 60 ks on September 7, 2001. The 8′ x 8′ field-of-view of a single CCD chip allows almost all of the galaxy to be imaged on the back-side-illuminated S3 chip. The raw data, with photons of pulse-height equivalent to energies below 0.3 keV or above 5 keV removed, are exhibited in Figure 1.

Source identification was done primarily with standard tools in the CIAO (*Chandra* Interactive Analysis of Observations) toolbox. `Celldetect` is a simple boxcar filter algorithm in the CIAO software package that utilizes a variable detection cell size (i.e., increasing with angular distance from the telescope aim point to match the telescope point spread function, PSF) that would include at least 80% of the counts from a point source. We applied the Celldetect algorithm to the 0.3-5 keV data of Figure 1, for which the algorithm detected 46 sources at a significance of $>3\sigma$. We separately applied the same algorithm to the data in several energy bands in order to perform some straightforward comparative diagnostics. There is a natural break in the X-ray response at 2 keV, which lends itself to defining the 2-5 keV band as hard (H). We have divided the softer X-rays into 0.3-0.5 (VS), 0.5-1 keV (S) and 1-2 keV (M). Sources that are detected in the VS band should be foreground sources since the X-ray optical depth through the Milky Way at 0.5 keV is $\sim$3.

We also utilized the `Vtpdetect` (Voronoi Tesselation and Percolation) algorithm, which considers asymmetric pixelation and can be more sensitive than Celldetect for point sources at the detection limit in uncrowded fields. Since 1″ corresponds to 30 pc at a distance of 5.9 Mpc, for this study we are more interested in the sensitivity of Vtpdetect than in the imaginative way that it might identify extended sources that would be tens or hundreds of pc in size. Vtpdetect identifies 86 sources at $>3\sigma$ when applied to the 0.3-5 keV FITS file of Figure 1. Visual inspection of the image results in 72 relatively firm identifications (at least 10 source counts). The typical background expectation in the southwestern portion of the image is less than 1 count, but in the northeast (where the point spread function is wider and there may be some diffuse emission) there may be as many as 3 background counts expected. In a separate study, Schlegel, Holt, & Petre (2002) are considering the extent to which this background might be diffuse emission in the galaxy associated with the hot phase of its interstellar medium. Other sources identified visually at slightly lower statistical confidence have not been included in Table 1 if they were not first objectively identified by Celldetect or Vtpdetect.

3. Characteristics of the Source Population

As an imaging spectrometer, the ACIS detector offers the opportunity to investigate the spatial, spectral and luminosity characteristics of the galactic source population.

Although we have not performed a quantitative correlation analysis, visual inspection of the location of

the X-ray sources projected on the optical image of NGC 6946 indicates a clear qualitative correlation with the spiral arms (Figure 2). A similar association was noted by Lacey & Duric (2001) for those radio sources that they designated to be "middle-aged SNR" (sources selected on the basis of their radio properties to be likely candidates for SNR with ages of $\sim 10^4$ years that are in the adiabatic phases of their expansion); 6 of the 35 sources in their sample are coincident (within 2″) with one of the 72 X-ray sources catalogued here. It should be noted that since the radio survey selected sources with nonthermal spectra (thermal radio SNRs are indistinguishable from H II regions), pulsar wind nebula SNRs with thermal radio spectra would not have been included in that survey. Interestingly, 8 of the 83 radio sources that do not meet the middle-aged SNR criteria were also coincident with X-ray sources. In particular, source 82 in the LDG radio catalog is coincident with the young remnant of SN1968D and is also identified with an X-ray source of 0.5-5 keV luminosity $\sim 3\times 10^{37}$ $(d_{5.9Mpc})^2$ erg s^{-1}. In contrast to the distribution of the middle-aged radio SNR, the 27 optically-selected SNR of Matonick & Fesen (1997) were not particularly well-correlated with the young stellar population of the spiral arms; here MF16 is the only member of the sample that has an X-ray counterpart.

The results of fits to the spectra of all those sources for which we have >300 counts are displayed in Table 2. All of these have inferred luminosities comparable to, or in excess, of the Eddington limit for a 1.4 $M_\odot$ neutron star ($L_{Edd} = 4\pi cGm_pM/\sigma_T = 1.3\times 10^{38}$ $M/M_\odot$ erg s^{-1}). Since the number of background counts accumulated in each spectrum is typically <10, we have not subtracted background in determining these fits. None of the spectra have the obvious bright K-lines that are associated with the ejecta of young (100-1000 year old) supernova remnants in the Milky Way, although some of the spectra can be described with optically thin thermal models that include less prominent line emission.

Of the 32 sources with >40 counts ($>2.8\times 10^{37}$ $(d_{5.9Mpc})^2$ erg s^{-1}), the general population appears to exhibit featureless "Crab-like" spectra. Comparing the S-M-H counts from each source with those expected from various power law trial spectra, half (16) are best characterized by $1.5< \Gamma <2.5$, with the other half evenly distributed between softer (7 with $\Gamma >2.5$) and harder (9 with $\Gamma <1.5$) spectra. The very brightest spectra seem, on average, to be slightly softer (see Table 2).

For source spectra that are not very steep (i.e., photon power law index $\Gamma \leq 2$ or energy power law index $\alpha \leq 1$, or models that have characteristic temperatures $\geq$ few tenths of a keV), column densities in the range $N_H = 3\text{-}5\times 10^{21}$ cm^{-2} typically reduce the source flux in the 0.5-5 keV band by about a factor of 2 relative to that which would be detected with $N_H = 0$. Using this prescription for typical source spectra, the minimum 0.5-5 keV source luminosity at 5.9 Mpc (corresponding to 10 counts) is approximately 7×10^{36} $(d_{5.9Mpc})^2$ erg s^{-1}, and the survey should be complete down to approximately 10^{37} $(d_{5.9Mpc})^2$ erg s^{-1}. More than a dozen sources have 0.5-5 keV luminosities comparable with, or in excess of, the Eddington luminosity for a 1.4 $M_\odot$ neutron star. Using the nearer distance to NGC 6946 would not substantially change this observation.

Figure 3 displays the traditional logN-logS distribution of the integral number of sources N(>S) with apparent luminosity greater than S. The unbinned distribution of the 72 sources detected with luminosities $>7\times 10^{36}$ $(d_{5.9Mpc})^2$ erg s^{-1} is well-fit with a power law index of 0.64±0.02 (95% confidence). If we confine the fit to luminosities $>10^{37}$ $(d_{5.9Mpc})^2$ erg s^{-1}, where we expect that the survey is complete, the fit steepens slightly to 0.68±0.03. The logN-logS distribution of the 20 sources with luminosities $>7\times 10^{36}$ $(d_{5.9Mpc})^2$ erg s^{-1} that are located within 2′ of the galactic center exhibit a somewhat flatter distribution, with an index 0.51±0.05. None of the sources in Table 1 appear to have either very soft (stellar-like) spectra or column densities much less than $N_H = 3\times 10^{21}$ cm^{-2}, so that all can either be associated with NGC 6946 or are background galaxies or AGN. Using the 0.7-2 keV logN-logS relationship of Ueda et al. (1999), which nicely overlaps the region of sensitivity for the sources that we detect in NGC 6946, we expect that the source list

of Table 1 should be contaminated with approximately 2 background sources. These contaminating galaxies would typically have the relatively hard spectra characteristic of AGN, but young pulsar-driven supernova remnants or X-ray binaries in NGC 6946 could have similarly hard spectra.

4. The Ultraluminous Source in NGC 6946

The X-ray source coincident with MF16 is the brightest X-ray source that we observe in NGC 6946, with 0.5-5 keV luminosity that we estimate to be approximately $8{\times}10^{39}$ $(d_{5.9Mpc})^2$ erg s^{-1}, based upon the two-component bremsstrahlung fit that is consistent with the average column density in the direction of NGC 6946. This is in good agreement with the luminosity estimated by Schlegel (1994) from data taken with *ROSAT*, but less than that estimated by Schlegel, Blair, & Fesen (2000) from data taken with *ASCA* (where the higher luminosity estimate might have arisen from over-correcting for the broad *ASCA* point spread function). Without clear evidence for a secular decrease in the MF16 luminosity, we shall assume that all three results are consistent with a constant source luminosity over ten years.

Schlegel, Blair, & Fesen (2000) have suggested that the morphology of MF16 region revealed by the *Hubble Space Telescope* (Blair, Fesen, & Schlegel 2001) could imply that the X-ray emission arises from the collision of shock fronts associated with multiple supernovae. The feature upon which this supposition rests is approximately 1″ in angular extent, which implies a blast wave cavity tens of pc in size. To traverse this distance, a blast wave of velocity 10^4 km s^{-1} would require $>10^4$ years, an age at which SNR blast waves are generally well past their free-expansion phases, and well past the times at which they would have exhibited their maximum luminosities. The 0.5-5 keV luminosity of MF16 is almost three orders of magnitude more than that of the brightest young blast wave remnants like Cas A.

It might be possible to explain the high luminosity in terms of a transient phase in the cooling, where the SN shock wave is depositing its kinetic energy into a dense ambient medium, since the emission measure is proportional to the square of the density. Such a scenario for this source has been suggested by Dunne, Gruendl, & Chu (2000), who argue that the characteristics of the source can be explained by supernova ejecta expanding into a dense nitrogen-rich circumstellar nebula created by the high-mass progenitor. However, as noted by the same authors, this cannot be the complete picture, since the spectrum measured by the *ROSAT* proportional counter requires a non-thermal contribution, perhaps from a pulsar or a pulsar wind nebula (or a superposition of more than one PWN). Moreover, the optically inferred blast wave velocity is less than 1000 km/s. With the current *Chandra* data, we see that the spectrum of MF16 is indisputably deficient in the line emission expected from an interaction with a dense CSM, although such a component could make a minor contribution to the overall spectrum.

The X-ray spectrum of MF16 has excellent statistics, containing several thousand counts. The lack of pronounced spectral features (such as the dominant K-lines that are characteristic of young blast-wave remnants) do not demand a unique model, and the spectrum can be fit equally well with a variety of models that sum two or more continuum components. One example is shown in Figure 4. This composite of a power law and thermal plasma (MEKAL in the jargon of the XSPEC fitting routine that was used here) might be consistent with a pulsar wind nebula and the interaction of the blast wave with a dense circumstellar shell, but both components are associated with unusually high luminosities that are not easily explained. Moreover, it is not the only model that gives an acceptable fit, and the two-component bremsstrahlung model has a higher column density that might better represent the unabsorbed continuum. The problem with the bremsstrahlung model is that it requires a very low ionization age to suppress the line emission, which is

not expected for a remnant that has been interacting with a dense circumstellar medium for at least the 10 years over which observations of this source have been made.

We find no evidence for the companion source that was reported by Schlegel, Blair, & Fesen (2000) at a level of 7% that of MF16 and at an angular distance 30″ from it . With no indication of a source at this position, its current level of emission must be at least an order of magnitude weaker than when detected by Schlegel, Blair, and Fesen, indicating that the missing source is likely to be a variable X-ray binary.

5. Galactic Nucleus

In the region of the galactic center, there are no sources coincident with the J2000 nuclear position RA=308.7201, DEC=60.1538 of Cotton, Condon, & Arbizzani (1999). Carignan et al. (1990) place the dynamical center some 5″ west of the Cotton, Condon, and Arbizzani position, coincident with the K′ peak reported by Regan & Vogel (1995). Two strong X-ray sources in the galactic center region are detected by the algorithms described in section 2, with the stronger source located ∼2″ south of the weaker. A third, much weaker source 11″ to the east is not detected by the algorithms (and not included in Table 1), although a fourth, yet weaker source to its south is detected, being far enough from the bright central region to be unaffected by the response of the telescope to other sources. The bright source lies ∼2.7″ NE (position angle ∼60 degrees E from N) from the dynamical center of Carignan et al. and ∼8.3″ W from the Cotton et al. center.

Both strong sources have spectra that are well-fit with power laws of energy index $\Gamma \sim 1.4$ with the same column density. This suggests the possibility that there may remain some contamination of our spectrum of the smaller by the larger, in spite of the fact that the two sources appear to be almost resolved; it could also indicate that the two sources have similar origins in the star-forming nucleus of the galaxy. Interestingly, the combination of the two sources appears very much like the morphology observed in both the CO image of Regan & Vogel (1995) and the H alpha image of Matonick & Fesen (1997) (see Fig. 6). The CO "molecular bar" is a roughly rectangular structure of dimensions approximately 60″ by 12″ including the central K′ (and H alpha) peak of Fig. 6 at a position angle of ∼135° E of N.

A similar central double source is found in a J−K image of the galactic center of NGC 6946 (Elmegreen, Chromey, & Santos 1998), but the sources are not coincident with the two strong central X-ray sources (see Figure 5 or 6). In fact, there is no correlation between the 14 J−K hot spots and the X-ray sources that we detect in the central region of the galaxy. The positions of the J-K hot spots, presumably associated with H II regions, are shown overlaid as circles on the Chandra image in Figure 5. The positions of the H II regions are inferred from the nuclear position given in the caption to Figure 11 of Elmegreen, Chromey, & Santos (1998), and are plotted twice: with squares using the Cotton et al. center, and with circles using the Carignan et al. center.

Although not easily discernible in Figure 5, but more easily visible in the contours of Figure 6, extended emission is present to the north and to the south; we are certain that this emission does not originate from the wings of the point spread function because it does not exhibit the PSF symmetry. Using the Carignan et al. position, the contours surround the nuclear H II region and the extended emission falls along the curve connecting the northern arm in the J−K image to the southern J−K extension. Using the Cotton et al. position, the contours lie W of the J−K center region and do not correspond to any structure in the J−K image.

6. Discussion

Luminous (>10^{36} erg s^{-1}) X-ray sources are most commonly degenerate stars accreting mass from non-degenerate companions in binary systems. The degenerate component of these binaries is typically a neutron star, since white dwarfs have insufficient surface gravity to provide luminous X-ray emission from accretion and stellar black holes in binaries appear to be relatively scarce. The masses of the non-degenerate binary components are used to classify X-ray binaries as high mass (HMXBs) or low mass (LMXBs), with the boundary in the relatively sparsely populated mass region of a few solar masses.

The X-ray LMXB and HMXB populations have now been characterized in several spiral galaxies, including the Milky Way. LMXBs have a dynamical lifetime (during which the system is not always X-ray-luminous) of order 10^{10} years, while the lifetime of HMXBs cannot exceed the nuclear timescale of the high mass components of the binary systems, or about 10^{7} years. Grimm, Gilfanov, & Sunyaev (2002a) have demonstrated that the HMXB luminosity of spiral galaxies exceeds the luminosity arising from LMXBs when the star formation rates (SFRs) exceed about 0.005 $M_{\odot}$ per year. X-ray luminous supernova remnants primarily arise from the same population of progenitors as HMXBs, but typically account for no more than a few percent of the HMXB luminosity (Helfand & Moran 2001). The timescales suggest that HMXBs and SNRs should be associated with star-forming regions in spiral arms and starburst nuclei, while LMXBs should be more uniformly distributed throughout the galactic bulges and haloes.

Grimm, Gilfanov, & Sunyaev (2002b) have confirmed that the distribution of X-ray binaries in the Milky Way conform to this general conventional wisdom, i.e., that the HMXBs are largely confined to the spiral arms, and that the LMXBs dominate the bulge (and total source) population, while having a larger scale height in the galactic plane. Grimm, Gilfanov, & Sunyaev (2002a,b) have also characterized the logN-logS distributions to be expected from LMXBs and HMXBs. The logN-logS distribution of HMXBs in both the Milky Way and in other galaxies of all types seems to have a "universal" index of 0.6 (for the integral distribution), with no evidence of a cutoff. The LMXB slope for the Milky Way is flatter (index 0.26) at low luminosities, but with a high luminosity cutoff that will steepen the apparent logN-logS precipitously if the low luminosity portion of the population is beyond the sensitivity of the survey. Kilgard et al. (2002) have suggested that an unbroken logN-logS index for starburst galaxies simply reflects the recent birth rate of HMXBs, while an aging population of LMXBs should exhibit a unit index break to accommodate the removal of sources at a characteristic age from an older population.

Recent results show that galaxies with star-forming rates similar to that of the Milky Way seem to exhibit similar characteristics. Tennant et al. (2001) report a steepening of the logN-logS distribution for the bulge of M81 for L_x >4×10^{37} ergs s^{-1} from a lower luminosity index of 0.5. A similar 0.5 index seems to characterize the disk population, but without a corresponding high luminosity steepening. It thus appears that the situation is much like that in the Milky Way, with LMXBs dominating the bulge and with HMXBs playing a larger role in the star-forming regions of the disk. The average source spectrum is consistent with a power law with Γ=1.6.

M31 seems to demonstrate at least some aspects of the same general behavior as M81 (Shirey et al. 2001; Trudolyubov et al. 2002; Kaaret 2002). The central region of the galaxy exhibits the high luminosity steepening characteristic of domination by LMXBs, while the outer regions of the galaxy exhibit an index of 1.2. While this is considerably steeper than 0.6, Trudolyubov et al. (2002) assign an origin in faint HMXBs to this population since the low luminosity index for LMXBs is even less compatible with the low luminosity index of LMXBs. Shirey et al. (2001) report an average source spectrum consistent with a power law with Γ=1.7.

In contrast, the results reported here for NCG 6946, i.e., for the entire galaxy (index 0.64) and for the central 2′ containing the starburst nucleus (0.51), are in good agreement with the expected 0.6 for HMXBs. The slightly flatter slope for the >2′ distribution may reflect a slightly higher contamination by bright LMXBs. The global SFR of NGC 6946 is more than an order of magnitude higher than that of the Milky Way, at approximately 4 $M_\odot$ yr^{-1} for stars in the mass range 2-60 $M_\odot$ (Sauty, Gerin, & Casoli 1998); most of this is in the outer spiral arms rather than the starburst nucleus.

M83 is a more intense starburst galaxy with a hotter and more compact photodissociation region than NGC 6946 (Israel & Baas 2001). Soria & Wu (2002) have reported that the central region surrounding the starburst nucleus has an X-ray logN-logS index of 0.8 (assumed by those authors to arise from continuous star formation), while the outer region is somewhat flatter (index 0.6) at low luminosities ($<6\times10^{37}$ ergs s^{-1})and steeper (index 1.3) at higher luminosities, so that most of the high luminosity population of the galaxy is in the central region. This might suggest that in M83 the HMXBs dominate the source population only in the central starburst region, rather than in the entire galaxy.

M101 is another face-on spiral galaxy which, like the others discussed above, has a typical H column density through the Milky Way that is as much as an order of magnitude lower than for NGC 6946. The global star formation rate for M101 is very similar to NGC 6946, at 4.8 $M_\odot$ yr^{-1}, a level about twenty times that of the Milky Way. The log N-log S distribution reported by Pence et al. (2001) is relatively flat (index of 0.8), and the X-ray sources are clearly associated with young population stars through their correlation with the spiral arms. The distribution of spectral indices for the sources is broad (per Figure 6 of Pence et al. 2001), with an average value similar to that of M81 or M31. Supersoft sources make up approximately 10% of the M101 sample, but this potential similarity with NGC 6946 cannot be tested, because the higher column density in the direction of NGC 6946 prevents their detection.

The global results reported here for NGC 6946 are consistent with the trends discussed above. With an SFR comparable to that of M101 and its characterization as a starburst galaxy, it should not be surprising that the distribution of X-ray sources in NGC 6946 matches that expected from a population dominated by HMXBs. The lack of obvious blast-wave SNRs may also be expected, in spite of the number of recent SNs, for at least two reasons. From the ratio of their X-ray-emitting lifetimes, the ratio of X-ray luminous SNRs to HMXBs originating in the same progenitor sample should be not much more than about 1%. Further, and most important in this study, a detection threshold at the level comparable to the luminosity of the Crab nebula will be incapable of detecting any but the very brightest members of the SNR population of NGC6946.

The galactic center region has two luminous X-ray sources close to the dynamical center. Since the luminosity of the southern member of the center pair is an order of magnitude in excess of that for an Eddington-limited neutron star, there is the suspicion that it might be associated with a central black hole. Although these two sources seem to fall on the central CO and H alpha images of NGC 6946, the other X-ray sources near galactic center do not cluster in the CO molecular bar or correlate in detail with H II regions identified by Elmegreen et al. in the central star-forming region of the galaxy.

The other NGC 6946 sources that exceed nominal neutron star Eddington luminosity can have their explanations in a variety of ways, such as magnetospheric effects around neutron stars, or black holes in place of neutron stars (e.g., see Grimm, Gilfanov, & Sunyaev 2002b). Kilgard et al. (2002) have noted that the presence of multiple super-Eddington X-ray sources seems to be characteristic of starburst galaxies, in marked contrast to non-starburst spirals. It is also interesting to note that stellar-mass black holes in the Milky Way have been identified with HMXBs that exhibit episodic X-ray increases (e.g., see Kong et al.

2002), so that we have local empirical evidence for the existence of black holes in HMXBs. A characteristic of such black hole sources is their spectral variability with luminosity phase; this latter variation may be the most efficient way to determine the nature of these sources in subsequent X-ray exposures to NGC 6946. If they are stellar black holes in HMXBs, the bright sources detected here are likely to be in the "high" states that usually exhibit spectra steeper than that of the Crab nebula; in this survey of NCG 6946 the most luminous sources appear to systematically exhibit spectra steeper than that of the Crab nebula, at least in the energy range 0.5-5 keV. Subsequent exposures to NGC 6946 that provide correlated spectral and intensity variations for these sources could provide the evidence that they are, indeed, black hole HMXBs.

The previous identification of the ultra-luminous source with the supernova remnant MF16 resulted in a plausible explanation for its high luminosity by Dunne, Gruendl, & Chu (2000) in terms of the cooling of a pre-SN circumstellar wind that has been recently heated by the SN blast wave (although it did not appear that it would be fully adequate and these authors suggested a possible additional pulsar component). A similar scenario had been invoked by Fabian & Terlevich (1996) to explain the detection of X-ray emission from SN1988Z 6.5 years after outburst with the *Rosat* High Resolution Imager (which has no energy resolution) at an inferred X-ray luminosity of $\sim 10^{41}$ ergs s^{-1}. The lack of prominent line emission in the current data is difficult to reconcile with this model, however. It is possible to contrive scenarios with pre-ionized circumstellar material to suppress line emission, but high luminosity arising from bremsstrahlung emission at high density will result in rapid cooling to temperatures at which X-ray line emission will be prominent. The apparent constancy of the luminosity for at least a decade and the lack of line emission argue against this being a complete explanation.

It may well be that the ultra-luminous source in NGC6946 has its ultimate explanation in a very unusual, if not a unique, set of circumstances. One possibility that might appear to have a relatively simple set of contrivances is a short-period pulsar with a high surface magnetic field. The 0.5-5 keV luminosity of the Crab nebula, with a central pulsar having a rotation period of 33 ms and an inferred surface magnetic field of the order of 10^{12} gauss, is approximately three orders of magnitude lower than that of MF16. Since the loss of pulsar rotational kinetic energy is proportional to the square of the surface field and the inverse fourth power of the period, a factor of three in both of these parameters relative to those of the Crab pulsar could provide a factor of 10^3 in luminosity. There are some obvious difficulties with this simple picture, however. There are no reported high-field pulsars with short periods or short-period spin-down pulsars with high fields (the fastest period for a pulsar in a remnant is 16 ms in N157B, with an inferred magnetic field of order 10^8 gauss, Marshall et al. 1998). The lack of a Crab-like gamma-ray source at the position of NGC 6946 (Hartman et al. 1999) is not particularly troublesome, since the distance to NGC 6946 would reduce the simple scaling of a source with gamma-ray luminosity 10^3 that of the Crab nebula to an apprarent luminosity of only 10^{-4}. A more serious difficulty with this explanation is that it demands a very young pulsar; we cannot sustain a very short pulsar period with a high luminosity that is the direct consequence of pulsar rotational energy loss. The implied characterisitic age for such a pulsar would be about 150 years, which is inconsistent with optical loop sizes of tens of pc and optical shock velocities of 600 km/s. We might reinvoke multiple SN to explain the optical characteristics of the region into which this anomalously bright pulsar was recently introduced, but the same coincidence could just have easily provided the setting for a HMXB with a massive stellar black hole. Future observations of the secular variation of the source intensity and/or spectrum should provide additional clues to the nature of this source.

7. Summary

We have utilized the *Chandra* ACIS imaging spectrometer to investigate the source population of the face-on galaxy NGC 6946. The gross aspects of the spatial and luminosity distributions of the source population suggest that HMXBs may play a significantly more important role here (relative to LMXBs) than in the Milky Way, consistent with the much higher SFR in NGC 6946. Although there are strong nuclear sources, including one that may be coincident with the center of the galaxy, there is no clustering of this sample in the CO molecular bar or correlation of the central X-ray sources with near IR "hot spots." The ten brightest sources in the galaxy appear to exceed the Eddington luminosity for a neutron star, and the very brightest, previously identified with a supernova remnant (MF16), exceeds it by two orders of magnitude. The most straightforward conjecture for the nature of all of these strong sources is that they are HMXBs with black hole degenerate members. In the case of MF16, the lack of strong X-ray emission lines in its X-ray spectrum suggests that the major fraction of its luminosity cannot be reconciled with traditional collisional models for the X-ray emission from supernova remnants.

Thanks to Olin undergraduate students Polina Segalova, Jessica Anderson, Anne Marie Rynning and Nicholas Zola for help with data extraction and analysis during the early phases of this study. The research of EMS was supported by contract number NAS8-38073 to SAO for the Chandra X-ray Center.

REFERENCES

Blair, W. P., Fesen, R. A., & Schlegel, E. M. 2001, ApJ, 121, 1497

Carignan, C., Charbonneau, P., Boulanger, F., & Viallefond, F. 1990, A&A 234, 43

Cotton, W. D., Condon, J. J., & Arbizzani, E. 1999, ApJS, 125, 409

deVaucouleurs, G. 1979, ApJ, 227, 729

Dunne, B. C., Gruendl, R. A., & Chu, Y.-H. 2000 AJ 119, 1172

Elmegreen, D. M., Chromey, F. R. & Santos, M. 1998, AJ, 116, 1221

Fabian, A. C. & Terlevich, R. 1996 MNRAS, 280, L5

Grimm, H.-J., Gilfanov, M., & Sunyaev, R. 2002a MNRAS (in press)

Grimm, H.-J., Gilfanov, M., & Sunyaev, R. 2002b A&A, 391, 923

Hartman, R. C. et al. 1999, ApJS, 123, 79

Helfand, D. J. & Moran, E. C. 2001, ApJ 554, 27

Israel, F. & Baas, F. 2001 A&A 371, 433

Kaaret, P. 2002, ApJ, 578, 114

Karachentsev, I. D., Sharina, M. E., & Huchtmeier, W. K. 2000, A&A, 362, 544

Kilgard, R. E., Kaaret, P., Krauss, M. I., Prestwich, A. H., Raley, M. T., & Zezas, A. 2002, ApJ, 573, 138

Kong, A. K. H., McClintock, J. E., Garcia, M. R., Murray, S. S., & Barret, D. 2002, ApJ, 570, 277

Lacey, C., Duric N., & Goss, W. 1997, ApJS, 109, 417

Lacey, C. K. & Duric, N. 2001, ApJ, 560, 719

Larsen, S. S., Efremov, Y. M., Elmegreen, B. G., Alfaro, E. J., Battinelli, P., Hodge, P. W., & Richtler, T. 2002, ApJ, 567, 896

Marshall, F. E., Gotthelf, E. V., Zhang, W., Middleditch, J., & Wang Q. D. 1998, ApJL, 499, L179

Matonick, D. M. & Fesen, R. A. 1997, ApJS, 112, 49

Pence, W. D., Snowden, S. L., Mukai, K., & Kuntz, K. D. 2001, ApJ, 561, 189

Regan, M. W. & Vogel, S. N. 1995, ApJL 452, L21

Sauty, S., Gerin, M., & Casoli, F. 1998, A&A, 339, 19

Schlegel, D. J., Finkbeiner, D. P., & Davis, M. 1998, ApJ, 500, 525

Schlegel, E. M. 1994, ApJ, 434, 523

Schlegel, E. M., Blair, W. P., & Fesen, R. A. 2000, AJ, 120, 791

Schlegel, E. M., Holt, S. S., & Petre, R. 2002, ApJ, in preparation

Shirey, R. et al. 2001, A&A, 365, L195

Soria, R. & Wu, K. 2002, A&A, 384, 99

Tennant, A. F., Wu, K., Ghosh, K. K., Kolodziejczak, J. J., & Swartz, D. A. 2001 ApJL, 549, L43

Trudolyubov, S. P., Borozdin, K. N., Priedhorsky, W. C., Mason, K. O., & Cordova, F. A., 2002, ApJL, 571, L17

Ueda, Y. et al. 1999, ApJ, 518, 656

Table 1: Detected Sources, Hardness Ratios, Identifications

	J2000		L_X	Source	Identities		
No.	RA	Dec	0.5-5 keV	Hardness	SBF[a]	LDG[b]	Comment
1	308.5357	+60.1712	10				
2	308.5792	+60.1689	62	M		1	
3	308.5890	+60.1716	30				
4	308.6029	+60.1774	48	H			
5	308.6039	+60.1517	170	M			
6	308.6088	+60.1527	700	M	S1		
7	308.6093	+60.1543	40				
8	308.6212	+60.1808	26				
9	308.6313	+60.1106	11				
10	308.6352	+60.1393	50	H			
11	308.6434	+60.1758	106	M/S	S2		
12	308.6470	+60.1285	16				
13	308.6503	+60.1443	42	S		17	
14	308.6515	+60.0995	33			18	
15	308.6520	+60.1584	810	M/S	S3		
16	308.6549	+60.1650	11				
17	308.6555	+60.1718	11				
18	308.6576	+60.0760	36				
19	308.6657	+60.1397	59	H		24	
20	308.6697	+60.1407	10				
21	308.6719	+60.1461	20			26	
22	308.6752	+60.0915	12				
23	308.6801	+60.1144	13				
24	308.6901	+60.1560	11				
25	308.6916	+60.1804	23				
26	308.6930	+60.2246	49	H/M			
27	308.6962	+60.1474	29				
28	308.6980	+60.1675	34			33	
29	308.6983	+60.1592	12				
30	308.7018	+60.1365	185	M			
31	308.7028	+60.1616	25				
32	308.7032	+60.0984	335	S	S4		
33	308.7043	+60.2049	210	M			
34	308.7064	+60.2286	24				
35	308.7071	+60.1699	20				
36	308.7072	+60.1699	25				

[a]sources from Schlegel, Blair, & Fesen (2000).

[b]sources from Lacey, Duric, & Goss (1997).

Table 1 (continued): Detected Sources, Hardness Ratios, Identifications

37	308.7076	+60.1349	13			43	
38	308.7077	+60.1721	10				
39	308.7085	+60.1568	41	M			
40	308.7104	+60.1710	10				
41	308.7116	+60.2019	11				
42	308.7120	+60.1294	15				
43	308.7121	+60.1725	66	S		48	
44	308.7149	+60.2139	12				
45	308.7180	+60.1533	780	M	S5		nucleus
46	308.7180	+60.1540	135	M			nucleus
47	308.7224	+60.1221	10				
48	308.7225	+60.1819	18			67	
49	308.7318	+60.1584	10				
50	308.7354	+60.1428	380	H/M	S6		
51	308.7356	+60.1387	25			79	
52	308.7367	+60.0923	46	H/M			
53	308.7405	+60.1636	340	M	S7		
54	308.7434	+60.1595	38			82	1968D
55	308.7440	+60.2382	84	H/M			
56	308.7505	+60.1522	1800	S	S9		
57	308.7527	+60.2139	43	H			
58	308.7531	+60.1919	8400	M/S	S10/8	85	MF16
59	308.7540	+60.1697	380	H/M	S11		
60	308.7581	+60.1676	170	H/M			
61	308.7692	+60.1882	73	M/S		91	
62	308.7697	+60.1551	15				
63	308.7722	+60.1064	90	H/M			
64	308.7770	+60.1781	15				
65	308.7830	+60.1871	15			101	
66	308.8033	+60.1254	191	H/M	S12		
67	308.8177	+60.1796	51	H			
68	308.8284	+60.1823	335	M	S13		
69	308.8335	+60.1597	15				
70	308.8380	+60.1644	25				
71	308.8561	+60.1665	78	S	S14?		
72	308.8661	+60.1553	36				

[a]sources from Schlegel, Blair, & Fesen (2000).

[b]sources from Lacey, Duric, & Goss (1997).

Table 2: Spectral Fit Results

Src ID[a]	Box (pixels[d])	Model[b]	χ^2/dof, dof	N_H ($\times 10^{22}$)	Γ or kT (- or keV)	Flux (10^{-13} erg s^{-1} cm^{-2}) Observed[c]	Source
6 (RA=308.609)	8×10	PL	1.36, 67	0.34 (0.27-0.44)	2.1 (1.9-2.3)	0.84	1.3
		Br	1.26, 67	0.25 (0.18-0.33)	3.6 (2.8-5.0)	0.87	1.1
15 (RA=308.652)	4×6	PL	1.22, 51	0.44 (0.33-0.51)	4.5 (4.0-5.0)	0.50	2.7
		Br	1.35, 51	0.16 (0.10-0.22)	0.69 (0.56-0.82)	0.50	0.81
32 (RA=308.703)	10×10	PL	1.82, 24	0.59 (0.37-0.85)	6.6 (5.2-8.3)	0.19	4.0
		Br	1.94, 24	0.32 (0.13-0.47)	0.27 (0.20-0.43)	0.18	0.78
		PSH[e]	1.37, 23	0.57 (0.52-0.69)	1.0 (0.51-1.9)	0.21	3.3
45 (RA=308.718)	12×12	PL	1.07, 85	0.60 (0.51-0.66)	2.6 (2.4-2.8)	1.1	2.8
		Br	1.05, 85	0.41 (0.36-0.47)	2.4 (2.0-2.8)	1.2	1.9
50 (RA=308.735)	6×6	PL	1.63, 28	0.78 (0.55-1.22)	1.78 (1.67-2.25)	0.43	0.77
		Br	1.60, 28	0.63 (0.44-0.94)	7.8 (4.0-16)	0.42	0.66
		PSH[f]	1.48, 27	0.83 (0.53-1.04)	5.9 (3.4-10.)	0.44	3.6
53 (RA=308.741)	8×10	PL	1.28, 28	0.64 (0.53-0.83)	2.8 (2.6-3.0)	0.32	0.90
		Br	1.27, 28	0.45 (0.32-0.59)	1.9 (1.6-2.5)	0.32	0.58
56 (RA=308.751)	10×12	PL	1.58, 85	0.52 (0.45-0.59)	4.9 (4.6-5.3)	1.2	9.3
		Br	1.84, 85	0.24 (0.19-0.29)	0.53 (0.46-0.61)	1.1	2.5
58 (RA=308.753)	14×20	PL	1.49, 204	0.15 (0.13-0.17)	2.44 (2.36-2.51)	7.1	9.8
		Br	1.90, 204	0.031 (0.019-0.043)	2.5(2.3-2.7)	7.1	7.5
		2Br	1.17, 202	0.42 (0.34-0.48)	3.2 (2.9-3.7)	4.7	7.4
					0.23 (0.20-0.27)	2.4	16.5
		MKL+PL	1.11, 202	0.12 (0.10-0.14)	kT=0.78 (0.63-0.84)	0.65	0.91
					Γ=2.2 (2.1-2.3)	6.3	8.0
59 (RA=308.754)	10×14	PL	1.10, 33	0.30 (0.21-0.50)	1.7 (1.5-2.0)	0.42	0.57
		Br	1.04, 33	0.27 (0.16-0.39)	6.8 (4.1-13.)	0.41	0.53
68 (RA=308.828)	24×24	PL	1.08, 38	1.2 (1.0-1.5)	3.1 (3.0-3.5)	0.52	2.6
		Br	0.86, 38	0.86 (0.70-1.07)	1.8 (1.4-2.1)	0.55	1.3

[a]Source number from Table 1.

[b]Models: PL=power-law; Br=bremsstrahlung; MKL=MEKAL; NEI=nonequilibrium ionization; PSH=plane-parallel shock

[c]Detected 0.5−5.0 keV flux

[d]1 ACIS pixel is 0.5″.

[e]Model sums ionization ages from 0 to $n_e t = 1.1(0.84 - 1.6) \times 10^{10}$ cm^{-3} s.

[d]Model sums ionization ages from 0 to $n_e t = 2.5(1.2 - 3.3) \times 10^{9}$ cm^{-3} s.

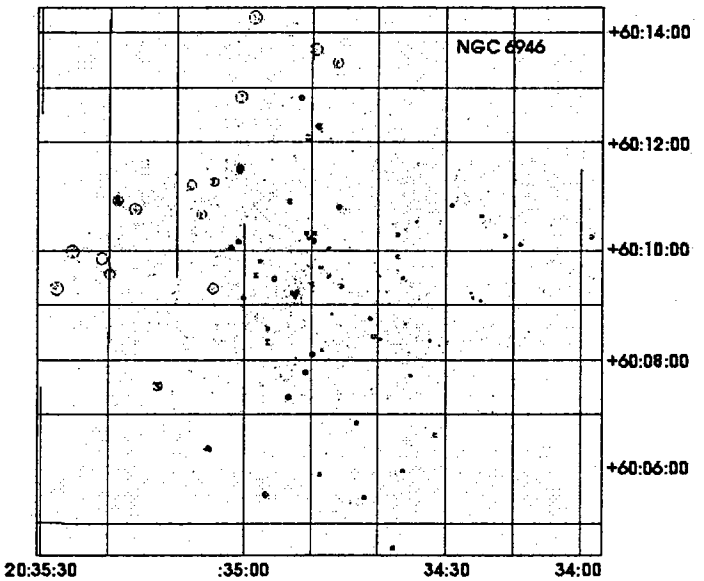

Fig. 1.— 60 ks *Chandra* observation of NGC 6946 on S3 ACIS chip (8 arc min on a side). Photons with energy-equivalent pulse height < 0.3 keV or > 5 keV are excluded.

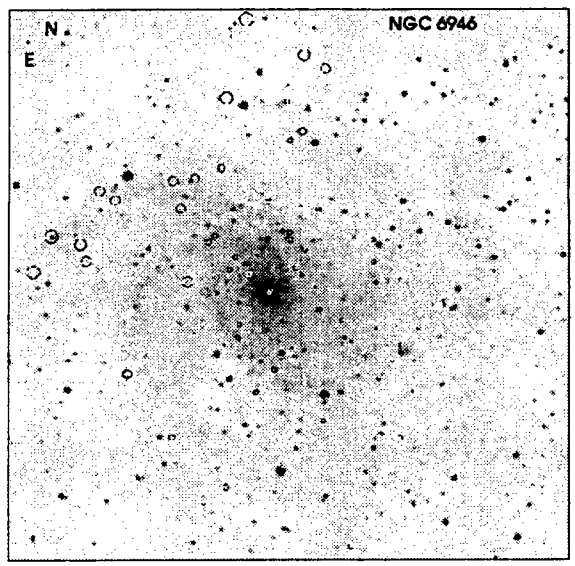

Fig. 2.— The 72 X-ray source positions displayed over the optical image of NGC 6946. Positional error circles increase with distance from the telescope aim point, which is approximately 3 arc minutes to the southwest of the galactic nucleus. The image is 8 arc min on a side.

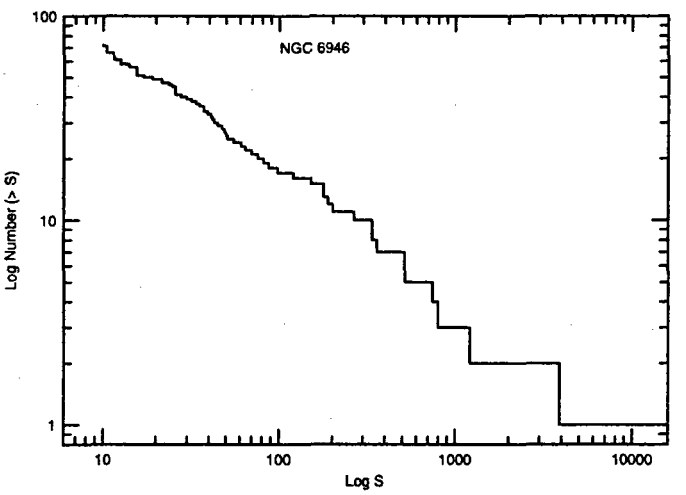

Fig. 3.— The integral logN/logs distribution of the 72 X-ray sources reported from this observation of NGC 6946. The horizontal scale has units of 7×10^{35} $(d_{5.9Mpc})^2$ erg s^{-1}.

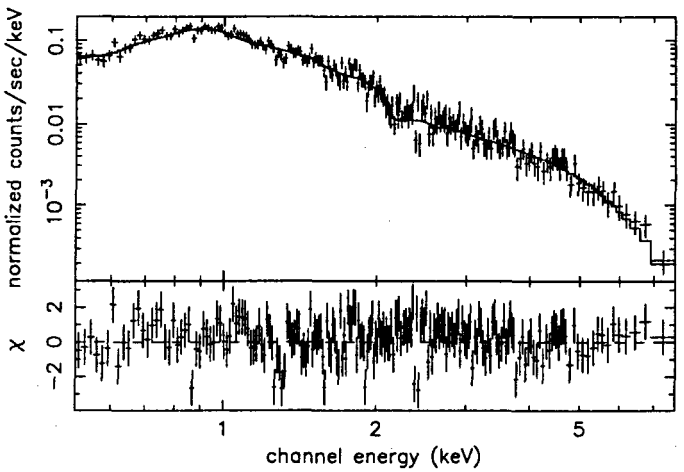

Fig. 4.— The X-ray spectrum of MF16. The model is a thermal plasma (MEKAL) and a power law, with column density only half of the average in the direction of NGC6946. A two-bremss model with higher column density is virtually indistinguishable. The fits are described in Table 2.

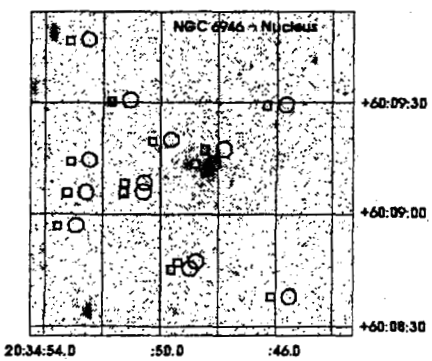

Fig. 5.— The inner region of NGC 6946. This region contains at two strong point sources, and several weaker ones. The symbols represent the nuclear H II regions described in Elmegreen, Chromey, & Santos (1998) but using two different definitions for the absolute center. The squares are referred to the center of Cotton, Condon, & Arbizzani (1999); the circles are referred to the center of Carignan et al. (1990).

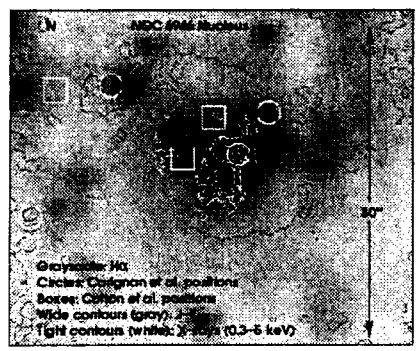

Fig. 6.— An expanded view of the nuclear region of NGC 6946. The grayscale is the Hα image from Matonick & Fesen (1997) overlaid with two sets of contours. The gray, wide contours represent J-K emission from Elmegreen, Chromey, & Santos (1998); the white contours represent 0.3-8 keV X-ray emission from the nucleus. The X-ray contours start at 2 counts pixel^{-1} and reach 20 counts pixel^{-1} in 5 logarithmic steps. The squares and circles are as in Figure 5, referring to the center defined by Cotton, Condon, & Arbizzani (1999) and Carignan et al. (1990), respectively.